Pump-probe spectroscopy of cold rubidium atoms in an integrating sphere

Wen-Li Wang,[1,2,*] Ri-Chang Dong,[1,3] Jian-Liao Deng,[1,†] and Yu-Zhu Wang[1]

[1]*Key Laboratory for Quantum Optics, Shanghai Institute of Optics and Fine Mechanics, Chinese Academy of Sciences, Shanghai 201800, China*

[2]*State Key Laboratory of Precision Spectroscopy, East China Normal University, Shanghai 200062, China*

[3]*University of Chinese Academy of Sciences, Beijing 100049, China*

(Received 24 January 2016; revised manuscript received 6 February 2016; published 5 May 2016)

Absorption spectra of cold rubidium atoms in an integrating sphere under the influence of a diffuse laser field have been systematically investigated. A pronounced dispersionlike structure centered at the light-shifted pump frequency is observed with a subnatural linewidth. In particular, two clearly resolved absorption resonances on the $5S_{1/2}(F = 2) \rightarrow 5P_{3/2}(F' = 3)$ transitions occur with variable probe beam intensity, which is consistent with our proposed theoretical model. Based on the two absorption resonances,we measure the dependence of light shifts, from which we can directly extract the effective Rabi frequency in a diffuse laser field, on the probe laser intensity, pump laser intensity, and pump laser detuning. Our work helps to identify the physical mechanisms behind these spectral features and is beneficial for studying the corresponding effect in a cold sample.

DOI: 10.1103/PhysRevA.93.052503

I. INTRODUCTION

To date, with the availability of high-power, tunable laser sources, various techniques have been proposed to exploit the behavior of the enhanced nonlinear atom-photon coupling system. Pump-probe spectroscopy, involving a coherent, single-frequency pump beam and a weak, scanned-frequency probe beam, has been widely used to extract information on a broad range of atomic species confined in optical lattices [1–3] and a magneto-optical trap (MOT) [4–14]. In theory, the absorption spectrum of a strongly driven two-level system was first calculated by Mollow [15] and developed by Cohen-Tannoudji *et al.* [16] using the dressed-atom model. Then, taking the degenerate levels and the polarization nature of the electromagnetic field into consideration, a numerical calculation model based on a density-matrix approach under weak or moderate pump field intensity [17–19] was proposed. Furthermore, numerous experimental studies have been devoted to cold atoms in an operating MOT. However, the presence of the fixed-dimensional geometry of the pump beams and the inhomogeneous trapping magnetic field impose restrictions on the flexibility of experimental arrangements, as well as the examination of the MOT spectra. On the other hand, atoms in an integrating sphere can also be cooled since the light from a proper incidence angle can automatically compensate Doppler shift of the moving atoms. Owing to the efficient cooling mechanism [20–25] and simple setup without the external magnetic fields, cold atoms in an integrating sphere are ideal candidates for studying the incident light polarizations, various physical process of the spectra, and broadening mechanisms. Such a process of diffuse laser cooling was first proposed by Wang in 1979 [26] and subsequently demonstrated by two experiments [27,28]. Recently several spectroscopic effects such as electromagnetically induced absorption (EIA) and recoil-induced resonance (RIR) have also been observed with cold atoms in diffuse laser light [29,30]. And the differences between the diffuse laser cooling and the optical molasses are also discussed. However, many physical mechanisms behind these nonlinear spectroscopy still have not been analyzed thoroughly; in particular, the corresponding theoretical models are required to nicely explain the observations in the integrating sphere.

In this paper, we experimentally and theoretically study pump-probe spectroscopy with cold Rb atoms in an integrating sphere. The diffusive cooling fields with arbitrary polarizations play the role of the pump field and propagate randomly with respect to the probe field. A pronounced dispersionlike structure at the light-shifted pump frequency is observed with a subnatural linewidth and two better-resolved absorption peaks. Due to the nonisotropic light shifts of the ground-state Zeeman sublevels in the probe laser field, two independent single-photon absorption resonances occur in our pump-probe spectra, which is different from the conventional optical molasses and MOT cases. Then the dependencies of light shifts on the probe intensity, pump intensity, and pump detuning are systematically investigated. Corresponding theoretical models based on different Raman processes in the integrating sphere are proposed and applied to interpret the observed spectral profiles. Our work helps to identify the physical mechanisms behind these different spectral features and provides important information on the atomic temperature [31–34], atomic cloud density [35], and effective Rabi frequency [36].

This paper is organized as follows. In Sec. II, we briefly describe our experimental setup. In Sec. III, we present in more detail our experimental results. The dependence of the spectral response features on different experimental parameters is systematically investigated and discussed. We present the model to describe these different spectral profiles in Sec. IV, and we conclude our work in Sec. V.

II. EXPERIMENTAL SETUP

The related energy levels of ^{87}Rb atoms with the excitations of the laser fields at wavelengths of 780 nm are shown in Fig. 1(a). The cooling (pump) and probe beams are derived from the same diode laser, whose frequency is locked to

*wangwenli@siom.ac.cn
†jldeng@siom.ac.cn

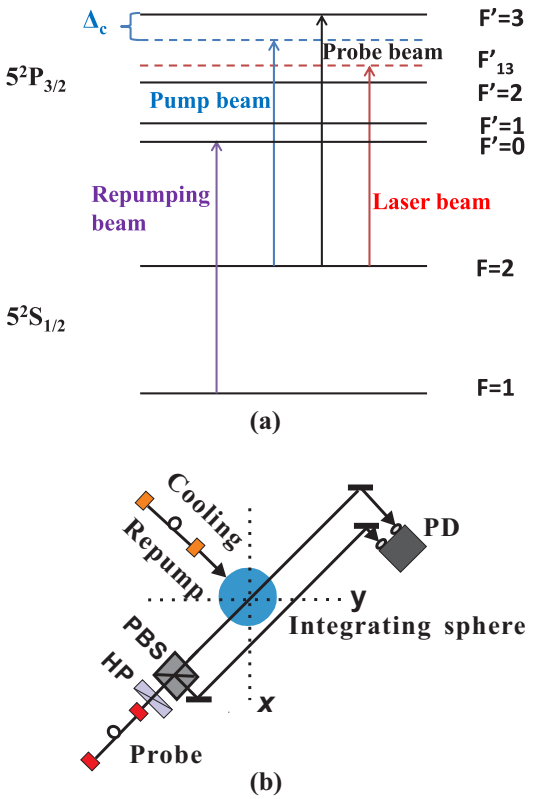

FIG. 1. (a) Energy levels of ^{87}Rb atoms with the relative excitations of the laser fields. The black and purple arrows symbolize the probe transition and the repumping transition, respectively. The laser beam is shown in red, locking to the center of the crossover line between the $5S_{1/2}(F=2) \rightarrow 5P_{3/2}(F'=1)$ and $5S_{1/2}(F=2) \rightarrow 5P_{3/2}(F'=3)$ transitions in saturated absorption spectroscopy. The pump beam is shown in blue, with a frequency offset Δ_c. (b) Schematic diagram of the experiment. HP, half-wave plate; PBS, polarized beam splitter; PD, photodiode. The pump beam overlapped with the repumping beam is injected into the integrating sphere through a single multimode fiber, while the probe beam is sent through a single-mode polarization-maintaining fiber. All beams propagate in the x-y plane.

the center of the crossover line between the $5S_{1/2}(F=2) \rightarrow 5P_{3/2}(F'=1)$ and $5S_{1/2}(F=2) \rightarrow 5P_{3/2}(F'=3)$ transitions of ^{87}Rb atoms in saturated absorption spectroscopy (SAS). We use 15 mW of a pump beam red-detuned to the cycling transition $5S_{1/2}(F=2) \rightarrow 5P_{3/2}(F'=3)$ by about 3Γ (where $\Gamma = 6.056$ MHz denotes the natural linewidth), and 0.5 mW of the $5S_{1/2}(F=1) \rightarrow 5P_{3/2}(F'=2)$ repumping beam. The frequency of the probe beam is scanned around the transition $5S_{1/2}(F=2) \rightarrow 5P_{3/2}(F'=3)$. Each laser frequency is individually detuned from the transition using an acousto-optic modulator (AOM).

A sample of cold ^{87}Rb atoms is produced by diffuse cooling inside an integrating sphere made from a coated spherical glass cell. The inner diameter of the integrating sphere is 48 mm, and the reflection coefficient is 0.96 for 780 nm. The pressure inside the glass cell is maintained at a level of 1×10^{-7} Pa with a 40 l/s ion pump. Figure 1(b) shows a schematic of the experimental apparatus. All beams propagate in the x-y plane. The pump beam overlapped with the repumping beam is injected into the integrating sphere through a single multimode fiber, while the probe beam is sent through a single-mode polarization-maintaining (PM) fiber. The latter is split into two beams with equal intensity by a half-wave plate (HP) and polarized beam splitter (PBS) combination; one passes through the cold atoms while the other is directly reflected in free space. The two beams fall onto a pair of photodiodes, and the differential signal is recorded and sent to a data acquisition system.

III. MEASUREMENTS AND RESULTS

In our experiment, the pump beam is always on; this keeps the atoms sufficiently cold for the measurements to be made, such that the observed spectra can be considered as steady state for the atoms without the presence of an external magnetic field. To understand the cooling mechanisms behind these spectral features in the integrating sphere, we first present a typical pump-probe spectroscopy that illustrates the characteristic features in the data. Then we present a series of spectra in which we vary the intensity of the probe field for a fixed intensity and detuning of the pump field. Different behaviors in the spectrum are discovered as the intensity increases, and the intensity dependencies of the light shift for cold atoms are measured. Finally, a series of spectra as a function of the pump frequency and the pump intensity is investigated, and a quantitative comparison of our results to the theoretical calculations is discussed.

A. Pump-probe spectroscopy in the integrating sphere

A representative transmission spectrum of cold ^{87}Rb atoms in the integrating sphere is shown in Fig. 2, where the powers of the probe and pump beams are 25 μW and 15 mW, respectively,

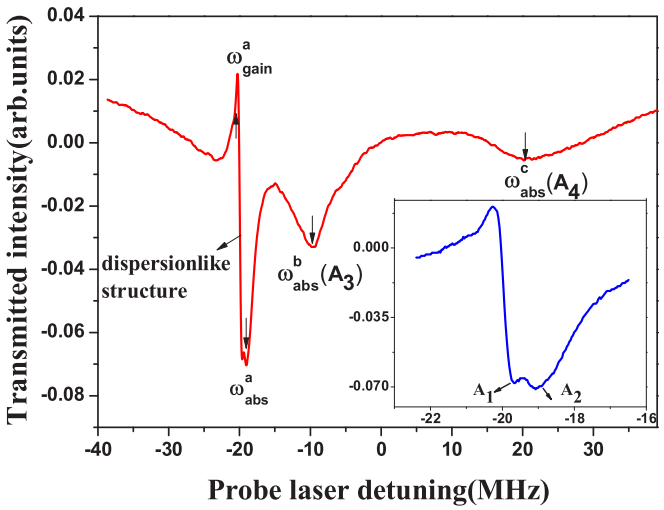

FIG. 2. A typical experimental pump-probe spectrum of cold ^{87}Rb atoms measured in the integrating sphere with a probe laser power of 25 μW, pump laser power of 15 mW, and detuning -18 MHz. Three resonances with different gain and absorption peaks, located at ω^a_{gain} (ω^a_{abs}), ω^b_{abs}, and ω^c_{abs}, are observed. Inset: Detailed information on the energy position of the dispersionlike structure. The absorption peak ω^a_{abs} has been decomposed into two peaks, A_1 and A_2.

and the pump detuning is −18 MHz. New spectral features characterized by a single dispersionlike structure centered at the middle point between the gain and absorption peaks with a subnatural linewidth and two independent line-absorption signals are observed. The energy positions of different gain peaks and absorption peaks are labeled as $\omega^a_{\rm gain}$ ($\omega^a_{\rm abs}$), $\omega^b_{\rm abs}$, and $\omega^c_{\rm abs}$, as shown in Fig. 2.

The pronounced dispersionlike structure in our experiment can be explained in terms of two physical mechanisms, which manifest themselves in the dispersive (RIR) and absorption (EIA) profiles. In fact, Zhang *et al.* [29] reported the coexistence of RIR and EIA for cold atoms in diffusive light, with the weak intensity of the probe laser beam of ∼20 μW/cm^2. However, from Fig. 2 it is clearly seen that, with the increased incident beam intensity ∼800 μW/cm^2, this dispersionlike structure can be better resolved, owing to the increases of the ac Stark shifts (light shift) of the ground-state sublevels. A detailed picture of the profile is shown in the inset and the absorption peak can be decomposed into two peaks. A quantitative description of the RIR and EIA signals can be found in Sec. IV. On the other hand, two independent line-absorption signals appear in the presence of the relatively intense probe beam instead of the single large absorption peak reported in Ref. [29], because of the splitting of the ground-state Zeeman sublevels. The larger width of these observed features is probably the consequence of the spatial inhomogeneity of the pump intensity. Next, we discuss the dispersionlike structure and the two small absorption peaks in detail.

B. Varying probe intensities

We present a series of pump-probe spectra in which we vary the intensity of the probe field, with the pump detuning and pump power fixed at −18 MHz and 15 mW, respectively, as shown in Fig. 3(a). In our measurement, the probe beam has a radius of 1 mm, and its frequency is scanned at 80 kHz/ms for a period of 1 s around the $5S_{1/2}(F=2) \rightarrow 5P_{3/2}(F'=3)$ transition. The probe beam power is selected by gradually increasing its value and monitoring its influence on the recorded spectra. We set different probe beam powers in the range from 0.4 to 452 μW, and the observed spectral features are significantly different from one another.

First, we discuss the dispersionlike structure, which is interpreted as a derivative signal (RIR) superposed on a pure absorption signal (EIA). As shown in Fig. 3(a), with increasing power of the probe beam, its amplitude grows significantly within the low probe power region. However, in the high probe power region, its linewidth is increased due to the power broadening effect, and thus the amplitude is decreased. Dependencies of the RIR center position and the EIA peak position on the probe laser power are plotted in Fig. 3(b), where the red stars represent the RIR center frequency and the blue diamonds represent the EIA peak frequency (A_1). We find that the RIR signals are nearly constant in frequency but differ from the frequency of the pump beam. Moreover, the peak position of the EIA signal varies as the probe beam power is increased due to the light-shift effect induced by the probe beam. These two contributions have different dependencies

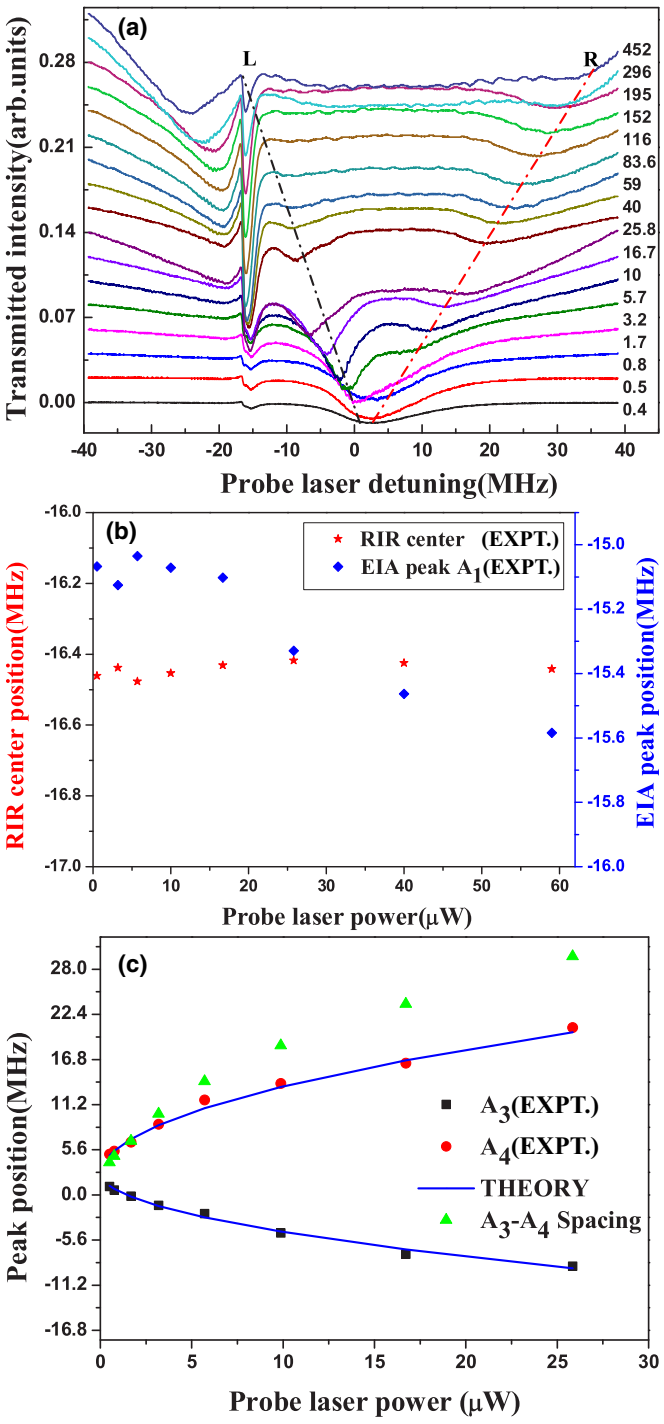

FIG. 3. (a) Pump-probe spectra recorded for different values of the probe laser power. The detuning of the pump field is −18 MHz, and the pump power is 15 mW. The L and R dashed lines indicate the two absorption peaks A_3 and A_4, respectively. (b) Dependence of RIR center positions (red stars) and EIA peak positions A_1 (blue diamonds) on the probe laser power. (c) Energy positions of the two absorption peaks (A_3, A_4) plotted as a function of the probe laser power. The red circles and black squares denote the experimental data and the solid lines are best-fit theoretical curves. The green triangles represent the spacing between the two absorption peaks.

on the probe beam power and we discuss different physical processes behind these spectra in the next section.

Second, we analyze the two resolved absorption resonances labeled L and R, which are associated with atomic linear absorption of the $5S_{1/2}(F = 2) \rightarrow 5P_{3/2}(F' = 3)$ transition as the probe power is increased. We also note that the energy positions of A_3 and A_4 varies in different directions with increasing probe power, and we plot the spectral features in Fig. 3(c). The black squares and red circles represent our experimental data, while the solid blue lines represent the best-fit theoretical results. A comparison of these measured data with the calculated light shift reveals good agreement between the experiment and theory. In addition, the green triangles represent the spacing between two absorption peaks, and the spacing becomes larger as the probe power increases, as shown in Fig. 3(c).

Third, we consider the light shift between the ground-state Zeeman sublevels owing to the pump and probe lasers. In our work, the light shift induced by the probe laser is comparatively large and cannot be ignored. For a fixed pump detuning of -3Γ and pump power 15 mW, the calculated light shift due to the pump laser is 2.8 MHz at a position when the probe power is zero, as shown in Fig. 3(c). Therefore, we can extract the correct values of the intensity or the Rabi frequency of the diffuse cooling light at the sites of the cold atoms inside the integrating sphere.

C. Varying pump detunings

Figure 4(a) illustrates the dependence of the pump-probe spectra on the detuning of the pump laser Δ_1 with fixed powers of the pump beam and probe beam, 15 mW and 25 μW, respectively. We note that the spectral behaviors are quite different from those in Fig. 3(a). First, the center frequency of the dispersionlike structure varies as the pump detuning increases, and it can be used as a precise marker of the position of the pump laser frequency. Second, the absorption signal in the dispersionlike structure is split into two absorption peaks, A_1 and A_2, for $\Delta_1 > \Gamma$ as depicted in the inset of Fig. 2. We illustrate such spectra of two absorption peaks as shown in Fig. 4(b), where the black stars and red triangles represent the measured energy positions of A_1 and A_2, respectively. One can observe that both sets of data exhibit linear behavior with increasing pump detuning and have similar values of slope. Third, the amplitude of the dispersionlike signal is initially enhanced with increasing pump detuning; then it is reduced once the detuning of the pump beam exceeds a certain value (-18 MHz in our case), due to the low efficiency of the diffusive cooling in the integrating sphere. There is an optimal pump detuning for the maximum amplitude of the dispersionlike structure. On the other hand, the energy positions of the two line-absorption peaks, marked with L and R, vary in a similar fashion to those in Fig. 3(a) as the pump detuning is increased. As shown in Fig. 4(c), as the pump detuning increases, the light shifts of both absorption peaks become larger, but with unequal magnitudes due to the different Clebsch-Gordan (CG) coefficients for each Zeeman sublevel in the ground state. The spacing between the two absorption peaks is also plotted in Fig. 4(c), which shows an increasing tendency as the pump detuning rises.

We present a summary of energy positions of these new spectral features for the series of experiments performed in

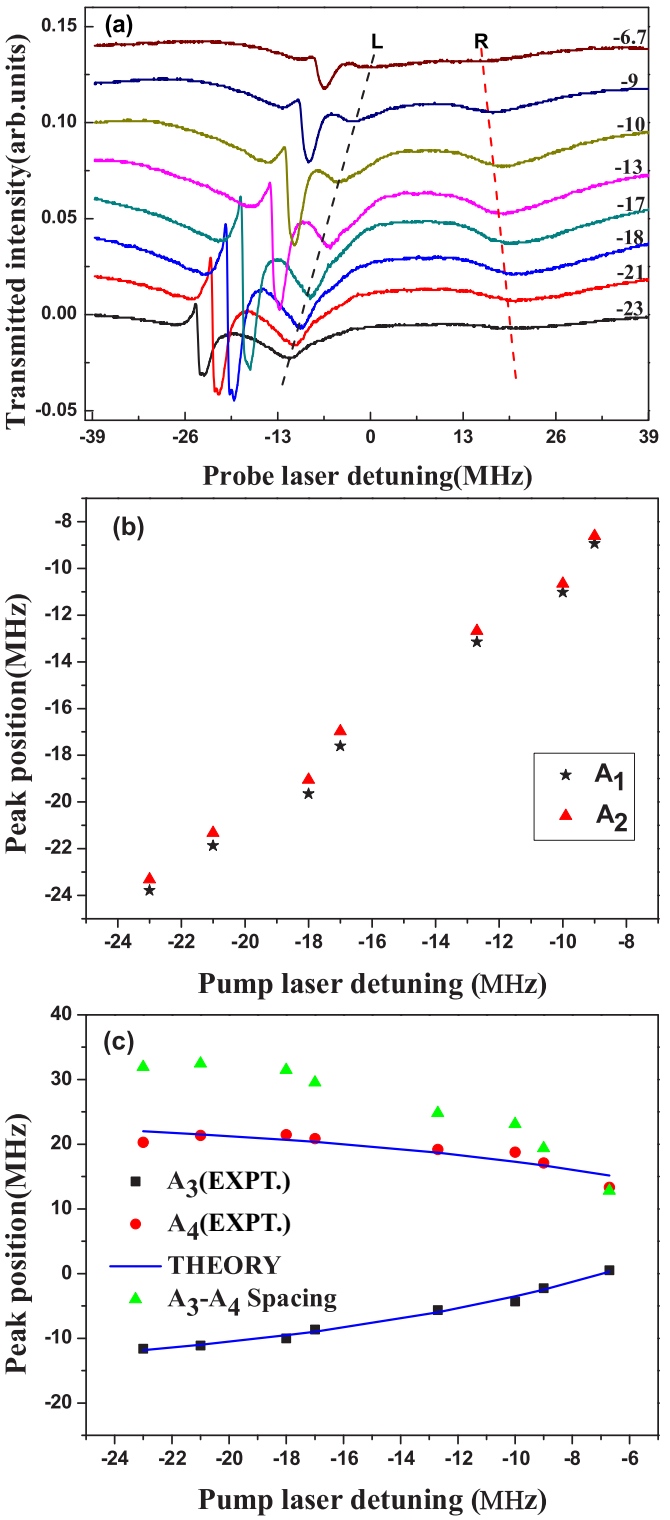

FIG. 4. (a) Pump-probe spectra recorded for different values of the pump laser detuning. The powers of the pump beam and probe beam are 15 mW and 25 μW, respectively. (b) Dependence of EIA peak positions A_1 and A_2 on the pump laser detuning. (c) Energy positions of the two absorption peaks (A_3, A_4) plotted as a function of the pump laser detuning. The notations are the same as in Fig. 3(c).

Table I. The gain and absorption peaks of the dispersionlike structure are labeled G_1, A_1, and A_2, respectively, while the

TABLE I. Experimental fitted energy positions from the spectra in Fig. 4 with various pump detunings Δ, and fixed pump laser power 15 mW. All the energy positions are with respect to the probe laser frequency and all quantities are in $2\pi \times$ MHz. The gain peak and absorption peak of the dispersionlike structure are labeled as G_1, A_1, and A_2, respectively, while the peaks of the two line-absorption resonances are labeled as A_3 and A_4.

Δ ($2\pi \times$ MHz)	$\omega^a_{\rm gain}(G_1)$ ($2\pi \times$ MHz)	$\omega^a_{\rm abs}(A_1)$ ($2\pi \times$ MHz)	$\omega^a_{\rm abs}(A_2)$ ($2\pi \times$ MHz)	$\omega^b_{\rm abs}(A_3)$ ($2\pi \times$ MHz)	$\omega^c_{\rm abs}(A_4)$ ($2\pi \times$ MHz)
−23	−24.2	−23.8	−23.3	−11.6	20.3
−21	−22.2	−21.9	−21.3	−11.1	21.4
−18	−20	−19.6	−19	−10	21.5
−17	−18	−17.6	−16.9	−8.7	20.9
−12.7	−13.7	−13.2	−12.7	−5.6	19.2
−10	−11.6	−11	−10.7	−4.3	18.8
−9	−9.6	−8.9	−8.6	−2.3	17.1

peaks of the two line-absorption resonances are labeled A_3 and A_4. As shown in Table I, we note that, with the detuning of −9 MHz, the gain and absorption peaks of the dispersionlike structure are distributed on both sides of the pump frequency; however, with the pump detuning increasing, their positions move to the left side of the pump frequency and the RIR center frequency obviously differs from the pump frequency as described in Refs. [7,29], due to the light shift induced by the probe and pump beams. The peak-to-peak distance of the dispersionlike structure is less than 1.2 MHz. As pump detuning is increased, the two line-absorption resonance signals move in the opposite direction with respect to the zero position, and their spacing becomes larger, as shown in Fig. 4(c) and Table I. Moreover, the broader widths of the experimentally observed features (not present in the table) indicate that some inhomogeneous broadening mechanisms may affect the spectra, for instance, the spatial inhomogeneity of the pump intensity, a stray dc magnetic field in the interaction region, recoil effect, and so on. We will present a detailed analysis in the future.

D. Varying pump intensities

Figure 5(a) shows the dependence of the observed spectra on the power of the pump beam. All scans are performed with the pump laser frequency tuned to the red side of the $5S_{1/2}(F = 2) \rightarrow 5P_{3/2}(F' = 3)$ transition with a fixed detuning of −18 MHz and the power of the probe laser is 25 μW. First, the amplitude of each spectrum, especially the two absorption signals, grows significantly with increasing the power of the pump beam, which indicates the variance of the population distribution in all atomic states due to the optical pumping effect. Second, the center position of the dispersionlike structure is independent of the pump laser power and stays at a fixed light-shifted pump frequency. Third, the two line-absorption peaks vary due to the light shift induced by the pump and probe beams. We measure the peak positions of the two line-absorption resonances from Fig. 5(a) and plot them as functions of pump laser power in Fig. 5(b). Really the energy positions of the two absorption peaks are varied according to the pump laser power in our experiment, and there is a linear scaling of the energy shift dependence. However, it should be noted that two line-absorption peaks vary in the opposite direction compared with the observations of Fig. 3(c), indicating the distinct cooling mechanism of our integrating sphere system that is different from the conventional MOT or optical molasses [37,38]. Therefore, an explicit measurement of the intensity dependence of the light shift in cold atoms

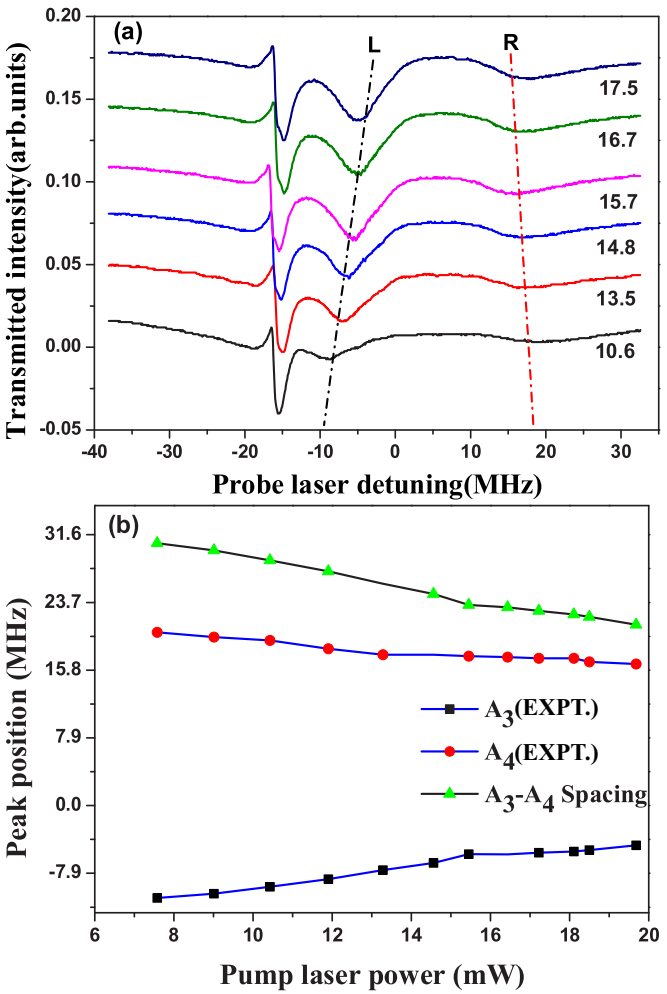

FIG. 5. (a) Pump-probe spectra recorded for different values of the pump laser power. (b) Energy positions of the two line-absorption peaks plotted as functions of the pump laser power. The detuning of the pump field is −18 MHz, and the probe power is 25 μW. The notation is the same as in Fig. 3.

seems to be of significant importance in this work. Presently, the analysis of the experimental results is complicated because of the various polarizations of the pump laser, the multibeam diffraction effect, and the intensity gradients at the site of atoms, and we are currently working to analyze this effect of various pump laser power.

IV. INTERPRETATION

The dispersionlike shape of the resonances observed experimentally in the integrating sphere reveals two physical mechanisms, which manifest themselves in the dispersive (RIR) and absorption (EIA) profiles. The theoretical calculation of both processes is presented below. Moreover, to explain the observed spectra of two line-absorption signals, a simple model for light shifts of a multilevel rubidium atom interacting with the incident light field is developed.

A. Recoil-induced resonance and electromagnetically induced absorption

RIR spectroscopy is associated with the two-photon Raman process between differently populated atomic momentum states [31,39–41]. A simple momentum-state calculation of RIR profile in the MOT and molasses cases can be found in Refs. [31,34,42]. In the integrating sphere, a detailed description of the RIR theoretical model can be found in our previous work [43], where the level degeneracy and uncertain polarization have been considered. In addition, the contributions of the momentum transfer, from the optical fields to the atoms and different atomic inner states, to the probe gain have been clearly indicated by our calculation. The calculated result of the RIR spectral profile is dispersive, and its width, defined as the peak-to-peak distance, is proportional to the temperature of the atomic cloud in the sphere. In fact, RIR has been used as a spectroscopic tool to measure the velocity distribution of the atoms cooled below the Doppler limit [31–33,43,44].

Next, let us consider the case of a driven degenerate two-level system on the cycling driven transition $F = 2 \rightarrow F' = 3$ in a ^{87}Rb atom inside the integrating sphere. The atom is subject to a weak probe beam with linear polarization and a strong pump beam with arbitrary polarizations (π, $\sigma^{\pm}$). Therefore, it is probable for the pump-probe configured EIA to occur, compared with the traditional MOT [45]. To the best of our knowledge, various polarization configurations of the pump and probe fields result in quite different spectra, which have been theoretically analyzed [19] and experimentally observed [8] in the MOT. In order to clarify the observed experimental results, we limit our consideration to the case where the pump field is circularly polarized and the probe field is linearly polarized in the direction parallel to the propagation direction of the pump field. The corresponding level structures of the D_2 line of ^{87}Rb and field schemes for a negative pump field detuning are shown in Fig. 6. Solid arrows represent the pump excitations and dashed arrows indicate the probe excitations. The size of the solid circle indicates the population distribution. The ac Stark splitting induced by the strong pump field and the population differences among the ground-state Zeeman levels are also represented. In this scheme, the optical

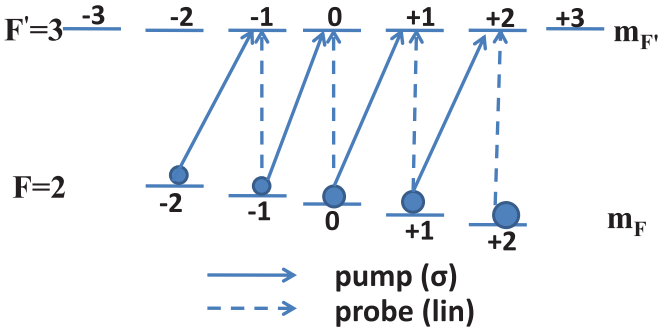

FIG. 6. Level structure for the strongly driven transition $F = 2 \rightarrow F' = 3$ in ^{87}Rb. The pump and probe polarizations are circular and linear parallel ($\sigma \parallel$ lin), respectively.

pumping leads to distribution of populations with the $m_F = 2$ sublevel being mostly occupied.

The EIA process is associated with Raman transitions between light-shifted Zeeman sublevels of the ground state [46–48]. Resonance occurs when the pump-probe detuning coincides with the energy separation of the adjacent sublevels. In our case, the EIA spectrum is obtained by summing the Lorentzian profiles over all allowed Raman transitions that depend on the polarization of the laser field, and it can be written as [10]

$$S_{\mathrm{EIA}}(\delta) = -\sum_{2}^{-2} w_{i,j} \triangle\pi_{i,j} L(\delta,\delta_{i,j},\gamma_{i,j}). \tag{1}$$

In the above equation, $\triangle\pi$ is the population difference between the relevant sublevels m_F, $w_{i,j}$ is the weight associated with the CG coefficients, and the Lorentzian profile is given by

$$L(\delta,\delta_{i,j},\gamma_{i,j}) = \frac{\gamma_{i,j}}{\gamma_{i,j}^2 + (\delta - \delta_{i,j})^2}, \tag{2}$$

where $\delta_{i,j}$ and $\gamma_{i,j}$ represent the resonance frequency and width of the $m_F = i \rightarrow m_F = j$ transition, respectively. Our model simplifies the cumbersome calculation of density-matrix element equations involved with multilevel atoms. From Eq. (1), we notice that the EIA spectral profile centers at the energy position equivalent to the light shift between the adjacent sublevels, and its amplitude is proportional to the products of the relevant population differences and the CG coefficients involved in the specific transition. As presented in Fig. 4(a), the resonance width is broadened, which is due to the spatial inhomogeneity of the light intensity in the integrating sphere and the presence of a stray magnetic field. Moreover, at high pump detunings, the EIA signal can be evolved into two absorption peaks, as shown in the inset of Fig. 2, since the values of the light shift between ground-state Zeeman sublevels become much larger.

B. Two resolved absorption resonances

Now we shift our attention to the two small absorption resonances, which are associated with atomic linear absorption of the $5S_{1/2}(F = 2) \rightarrow 5P_{3/2}(F' = 3)$ transition. We explicitly report measurements of the intensity and detuning dependence of the light shift using this spectral feature for cold Rb atoms inside the integrating sphere. Similar to the

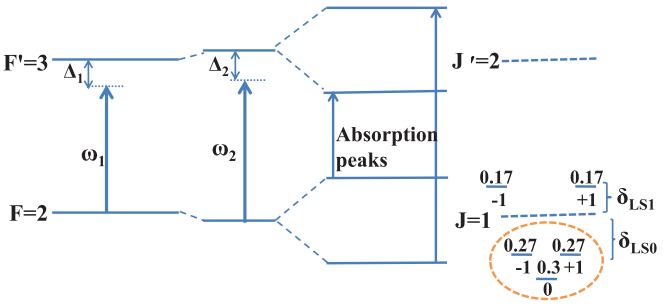

FIG. 7. Modeling the ^{87}Rb atom as a fictitious $J = 1 \rightarrow J' = 2$ system with two coupling fields. Here, ω_1 and Δ_1 represent the frequency and detuning for the first coupling field (pump) acting on the bare atomic levels when $\Delta_1 < 0$, and ω_2 represents the frequency for the second coupling field (probe) acting on the dressed levels with a detuning Δ_2. Values on each Zeeman sublevel in the ground state are the squared CG coefficients. δ_{LS0} and δ_{LS1} denote the relative size of the light shift for each sublevel.

treatment of the two-level dressed atom approach [7,13,49,50], the corresponding theoretical model for a multilevel atom in ^{87}Rb with two coupling fields is depicted in Fig. 7. Here, ω_1 represents the frequency of the pump field for the negative detuning case $\Delta_1 < 0$ acting on the bare atomic levels, and ω_2 represents the frequency of the strong probe field acting on the dressed levels with a detuning $\Delta_2 > 0$ or $\Delta_2 < 0$. The dashed horizontal line indicates the unperturbed energy level and the values on each light-shifted Zeeman sublevel are the squared CG coefficients. As shown in Fig. 7, the encircled three sublevels are close lying, such that we approximate them as one with an average squared-CG coefficient of 0.28 and effectively model the Rb atom as a $J = 1 \rightarrow J' = 2$ system [51]. Now that the ground state of $J = 1$ has been split into two sublevels, two transitions are possible, as shown by the arrows, and are characterized by the absorption peaks near ω_2 in Fig. 7. As expected in Fig. 2, two absorption-peak resonances corresponding to the $F = 2 \rightarrow F' = 3$ transition are observed as a function of probe frequency. One peak is located around the red-detuned frequency of the probe laser, and the other the blue-detuned frequency.

The light shift for any one of the Zeeman ground states is given by [51]

$$(\delta_{\mathrm{LS}})_{m_F} = \frac{\left(\Delta_2 - \sqrt{\Delta_2^2 + \Omega_2^2}\right)}{2} |c_{m_F} c_{m'_F}|^2, \qquad (3)$$

where Δ_2 is the detuning of the probe beam, Ω_2 is the corresponding Rabi frequency, and $c_{m_F m_F}$ is the CG coefficient for the transition between the ground state m_F and the excited state m'_F. For the $J = 1 \rightarrow J' = 2$ system, the relative light shift between the ground states is denoted by δ' and given by

$$\delta' \equiv (\delta_{\mathrm{LS}})_{m_F=0} - (\delta_{\mathrm{LS}})_{m_F=\pm 1}. \qquad (4)$$

For a fixed detuning of the probe laser, the relative light shift, induced by the probe laser alone, calculated from Eq. (3) gradually grows larger as the probe beam intensity increases. However, for either a negative or positive probe detuning, two sublevels of the ground state $J = 1$ are shifted toward $\delta' = 0$ in opposite directions, which leads to a widening difference of the two light shifts according to Eq. (4) as the probe intensity rises. Meanwhile, the energy positions of the two absorption profiles, corresponding to the different sublevels between the $J = 1 \rightarrow J' = 2$ transition, measured in Figs. 3 and 4 vary in opposite directions as a function of the probe intensity or pump detuning. A comparison of these light-shift data obtained for the integrating sphere with the calculated values reveals good agreement between experiment and theory. On the other hand, for strong pump intensity, the total energy level shift in Fig. 5(b), arising from the pump and probe lasers, varies in a significantly opposite way compared with those in Figs. 3 and 4. We preliminarily speculate it may be caused by the unique characteristics of diffuse laser light inside an integrating sphere [43]. The light shifts shown here for cold atoms inside an integrating sphere measured as a function of intensity are quantitatively different from the case of a traditional MOT or molasses reported. The details of both our analytic calculations and experimental results about the effect of pump laser power will be presented elsewhere. Moreover, taking the beam divergence and the estimated losses into account, the pump intensity at the sites of cold atoms within the integrating sphere is difficult to determine. In this work, using the light shift in cold-atom measurements combined with the proposed theoretical model, we can extract the correct value of the pump intensity or its average Rabi frequency.

V. CONCLUSION

In summary, we have systematically investigated the pump-probe spectroscopy for cold atoms in an integrating sphere. A pronounced dispersionlike structure with two better-resolved absorption peaks and two interesting line-absorption resonances are observed and their behaviors are nicely explained by our proposed theoretical models. The dependencies of light shifts on probe laser intensity, pump laser intensity, and detuning are measured, respectively. Our work helps to explore the physical mechanisms behind these experimental observations and provides a powerful spectroscopic tool to extract information about cold atoms, such as atomic temperature, atomic density, and especially the effective Rabi frequency of the diffuse laser field interacting with the atoms inside the integrating sphere. In addition, this technique is beneficial for improving the performance of the integrating sphere atomic clock.

ACKNOWLEDGMENTS

This work is supported by the National Natural Science Foundation of China under Grants No. 11404353 and No. 91536220, and the Open Research Fund of the State Key Laboratory of Precision Spectroscopy (East China Normal University).

[1] G. Grynberg and C. Robilliard, Phys. Rep. **355**, 335 (2001).

[2] M. Brzozowska, T. M. Brzozowski, J. Zachorowski, and W. Gawlik, Phys. Rev. A **73**, 063414 (2006).

[3] B. Deissler, K. J. Hughes, J. H. T. Burke, and C. A. Sackett, Phys. Rev. A **77**, 031604 (2008).

[4] D. Grison, B. Lounis, C. Salomon, J. Y. Courtois, and G. Grynberg, Europhys. Lett. **15**, 149 (1991).

[5] J. W. R. Tabosa, G. Chen, Z. Hu, R. B. Lee, and H. J. Kimble, Phys. Rev. Lett. **66**, 3245 (1991).

[6] B. Lounis, J.-Y. Courtois, P. Verkerk, C. Salomon, and G. Grynberg, Phys. Rev. Lett. **69**, 3029 (1992).

[7] M. Mitsunaga, T. Mukai, K. Watanabe, and T. Mukai, J. Opt. Soc. Am. B **13**, 2696 (1996).

[8] Y. C. Chen, Y. W. Chen, J. J. Su, J. Y. Huang, and I. A. Yu, Phys. Rev. A **63**, 043808 (2001).

[9] S. Y. Zhou, Z. Xu, S. Y. Zhou, and Y. Z. Wang, Chin. Phys. Lett. **22**, 1672 (2005).

[10] T. M. Brzozowski, M. Brzozowska, J. Zachorowski, M. Zawada, and W. Gawlik, Phys. Rev. A **71**, 013401 (2005).

[11] M. Brzozowska, T. M. Brzozowski, J. Zachorowski, and W. Gawlik, Phys. Rev. A **72**, 061401 (2005).

[12] J. A. Greenberg and D. J. Gauthier, Phys. Rev. A **79**, 033414 (2009).

[13] Y. P. Ruan, F. D. Jia, Z. Sun, S. F. Lv, B. Qing, W. Huang, P. Xue, X. Y. Xu, X. C. Dai, and Z. P. Zhong, Phys. Rev. A **90**, 033811 (2014).

[14] H. J. Fu, J. B. Tan, P. C. Hu, and Z. G. Fan, Chin. Opt. Lett. **13**, 101201 (2015).

[15] B. R. Mollow, Phys. Rev. A **5**, 2217 (1972).

[16] C. Cohen-Tannoudji and S. Haroche, J. Phys. **30**, 125 (1969); J. Phys. B **10**, 345 (1977); C. Cohen-Tannoudji, in *Frontiers in Laser Spectroscopy*, edited by R. Balian, S. Haroche, and S. Liberman (North-Holland, Amsterdam, 1977).

[17] A. Lezama, S. Barreiro, and A. M. Akulshin, Phys. Rev. A **59**, 4732 (1999).

[18] A. Lezama, S. Barreiro, A. Lipsich, and A. M. Akulshin, Phys. Rev. A **61**, 013801 (1999).

[19] A. Lipsich, S. Barreiro, A. M. Akulshin, and A. Lezama, Phys. Rev. A **61**, 053803 (2000).

[20] E. Guillot, P. E. Pottie, and N. Dimarcq, Opt. Lett. **26**, 1639 (2001).

[21] X. C. Wang, H. D. Cheng, L. Xiao, B. C. Zheng, Y. L. Meng, L. Liu, and Y. Z. Wang, Chin. Opt. Lett. **10**, 080201 (2012).

[22] B. C. Zheng, H. D. Cheng, Y. L. Meng, L. Xiao, J. Y. Wan, and L. Liu, Chin. Phys. Lett. **30**, 123701 (2013).

[23] H. D. Cheng, W. Z. Zhang, H. Y. Ma, L. Liu, and Y. Z. Wang, Phys. Rev. A **79**, 023407 (2009).

[24] F. X. Esnault, D. Holleville, N. Rossetto, S. Guerandel, and N. Dimarcq, Phys. Rev. A **82**, 033436 (2010).

[25] F. X. Esnault, N. Rossetto, D. Holleville, J. Delporte, and N. Dimarcq, J. Adv. Space Res. **47**, 854 (2011).

[26] Y. Z. Wang, in Proceedings of the National Symposium on Frequency Standards, Chengdu, China, 1979 (unpublished).

[27] W. Ketterle, A. Martin, M. A. Joffe, and D. E. Pritchard, Phys. Rev. Lett. **69**, 2483 (1992).

[28] H. Batelaan, S. Padua, D. H. Yang, C. Xie, R. Gupta, and H. Metcalf, Phys. Rev. A **49**, 2780 (1994).

[29] W. Z. Zhang, H. D. Cheng, L. Liu, and Y. Z. Wang, Phys. Rev. A **79**, 053804 (2009).

[30] W. Z. Zhang, H. D. Cheng, L. Xiao, L. Liu, and Y. Z. Wang, Opt. Express **17**, 2892 (2009).

[31] J.-Y. Courtois, G. Grynberg, B. Lounis, and P. Verkerk, Phys. Rev. Lett. **72**, 3017 (1994).

[32] D. R. Meacher, D. Boiron, H. Metcalf, C. Salomon, and G. Grynberg, Phys. Rev. A **50**, R1992 (1994).

[33] G. Di Domenico, G. Mileti, and P. Thomann, Phys. Rev. A **64**, 043408 (2001).

[34] M. C. Fischer, A. M. Dudarev, B. Gutierrez-Medina, and M. G. Gaizen, J. Opt. B **3**, 279 (2001).

[35] A. Lezama, G. C. Cardoso, and J. W. R. Tabosa, Phys. Rev. A **63**, 013805 (2000).

[36] J. Zachorowski, T. Brzozowski, T. Palasz, M. Zawada, and W. Gawlik, Acta Phys. Pol. A **101**, 61 (2002).

[37] K. Kim, M. Kwon, and J. B. Kim, J. Opt. Soc. Korea **5**, 131 (2001).

[38] M. Glodz, K. Kowalski, E. Paul-Kwiek, and J. Szonert, Opt. Commun. **284**, 3292 (2011).

[39] J. Guo, P. R. Berman, B. Dubetsky, and G. Grynberg, Phys. Rev. A **46**, 1426 (1992).

[40] J. Guo and P. R. Berman, Phys. Rev. A **47**, 4128 (1993).

[41] P. R. Berman, B. Dubetsky, and J. Guo, Phys. Rev. A **51**, 3947 (1995).

[42] P. Verkerk, in *Coherent and Collective Interactions of Particles and Radiation Beams*, Proceedings of the International School of Physics "Enrico Fermi," Course CXXXI, Varenna, 1996, edited by A. Aspect, W. Barretta, and R. Bonifacio (IOS Press, Amsterdam, 1997), p. 325.

[43] W. L. Wang, J. L. Deng, and Y. Z. Wang, J. Opt. Soc. Am. B **32**, 2441 (2015).

[44] L. V. Il'ichev, JETP Lett. **86**, 167 (2007).

[45] C. Goren, A. D. Wilson-Gordon, M. Rosenbluh, and H. Friedmann, Phys. Rev. A **67**, 033807 (2003).

[46] A. M. Akulshin, S. Barreiro, and A. Lezama, Phys. Rev. A **57**, 2996 (1998).

[47] A. V. Taichenachev, A. M. Tumaikin, and V. I. Yudin, Phys. Rev. A **61**, 011802(R) (1999).

[48] Y. C. Chen, C. W. Lin, and I. A. Yu, Phys. Rev. A **61**, 053805 (2000).

[49] C. Cohen-Tannoudji, J. Dupont-Roc, and G. Grynberg, *Atom-Photon Interactions: Basic Processes and Applications* (Wiley, New York, 1992).

[50] G. Grynberg and C. Cohen-Tannoudji, Opt. Commun. **96**, 150 (1993).

[51] N. Souther, R. Wagner, P. Harnish, M. Briel, and S. Bali, Laser Phys. Lett. **7**, 321 (2010).